Satellite Observations of Upwelling in the Gulf of Guinea

George Wiafe and Ebenezer S. Nyadjro

***Abstract*—The classical case of favorable winds driving coastal upwelling does not adequately account for the upwelling observed along the northwestern Gulf of Guinea (GoG) coast, which is the area of focus in this letter. Herein, we used mainly satellite-derived data to examine the dynamics of upwelling in the study area. Upwelling indexes are derived from sea surface temperature (SST) and wind influences. Low SST, which is a characteristic of upwelling, is observed mainly along the entire coastal region from July to September. The relative contributions of local wind forcing are quantified; the wind-stress-driven Ekman transport was more important than the wind-stress-curl-driven Ekman pumping in affecting changes in SST. They both however do not entirely explain the upwelling that is observed along the entire coast. It is shown that winds in the western equatorial Atlantic force eastward propagating upwelling Kelvin waves that lead to lowering of sea level and SST along the northwestern GoG coast.**

***Index Terms*—Altimetry, Ekman transport, Gulf of Guinea, Kelvin waves, satellite data, sea surface temperature (SST), upwelling, winds.**

I. Introduction

THE occurrence of upwelling in coastal waters is important for local ecosystems as cold nutrient-rich waters are brought into the surface ocean, which in turn enhance biological productivity. The Central and Eastern Atlantic experience two main upwelling phenomena: coastal and equatorial upwelling. In the northwestern Gulf of Guinea (GoG), the coastal waters between Côte d'Ivoire and the Republic of Benin [see Fig. 1(a)] experience two periods of upwelling: minor and major upwelling. The minor phenomenon typically lasts about three weeks and occurs at any time between December and March, whereas the major phenomenon consistently occurs between July and September [1]–[3]. In the Guinea current, upwelling has a significant effect on the abundance of fish and the rainfall distribution along the western African coast and the sub-Saharan countries. The low sea surface temperatures (SSTs) during an upwelling tend to inhibit convection, which does not favorably allow moisture convergence over the African continent by the southwesterly winds [4]–[6]. Consequently, understanding the variability in intensities of upwelling along the coasts of the GoG is of great interest to both meteorologists and oceanographers.

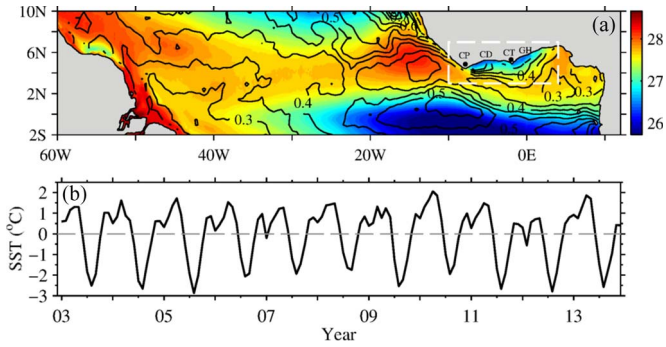

Fig. 1. (a) Annual mean SST (in degrees Celsius) (color shaded) in the Central Atlantic Ocean. Contours show standard deviation of SST. Contour interval is 0.05 °C. White box (10° W–4° E, 3° N–7° N) shows the northwestern GoG region, our primary area of focus: CP, Cape Palmas; CD, Côte d'Ivoire; CT, Cape Three Points; GH, Ghana. (b) Seasonal variation of SST spatially averaged in the northwestern GoG box region from 2003 to 2013.

The classical case of coastal upwelling suggests that winds parallel to the coastline will cause a net surface water mass transport (Ekman transport) to the right of the wind direction in the Northern Hemisphere (to the left in the Southern Hemisphere) due to the Coriolis effect. To maintain mass balance, this divergence leads to an upward motion of cold nutrient-rich water below the thermocline into the surface layer [7]. The resulting changes in the surface waters include a drop in SST, low oxygen, and increased primary productivity [1]. The drop in SST, in particular, is often used as an indicator of upwelling. This makes satellite-derived data useful in studying the dynamics of coastal upwelling [8].

The climate system in the GoG is largely influenced by wind variability and the seasonal migration of the Intertropical Convergence Zone (ITCZ). Southeast winds are dominant in the boreal summer when the ITCZ lie in its northern position. During this time, the southeasterly winds carry moisture-laden air over West Africa and the Sahel, leading to high precipitations. During boreal winter, dry northeasterly winds dominate, whereas the southeasterly winds weaken. These northeasterly winds carry Harmattan dust over the whole of West Africa. At this time, the ITCZ retreats southward, leading to cessation of rains on the African subcontinent [5], [9].

Earlier studies of upwelling in the Guinea current have suggested varied mechanisms for the occurrence of the upwelling. Hypotheses proposed in the 1970s and 1980s to explain the upwelling, although still contentious today, include wind-driven Ekman divergence [10], geostrophic-induced upwelling [9],

Manuscript received September 2, 2014; revised November 25, 2014; accepted December 4, 2014. E. S. Nyadjro was supported by a National Research Council Research Associateship award at the National Oceanic and Atmospheric Administration/Pacific Marine Environmental Laboratory. This is PMEL contribution no. 4248.

G. Wiafe is with the Department of Marine and Fisheries Sciences, University of Ghana, Accra, Ghana.

E. S. Nyadjro is with National Oceanic And Atmospheric Administration Pacific Marine Environmental Laboratory, Seattle, WA 98115 USA (e-mail: ebenezer.nyadjro@noaa.gov).

Color versions of one or more of the figures in this paper are available online at http://ieeexplore.ieee.org.

Digital Object Identifier 10.1109/LGRS.2014.2379474

cape-interaction [11], and remotely forced coastally trapped waves [12]. Some authors [13], [14] argued that the local wind forcing might account for the variability in the upwelling, whereas [15] suggested that remote forcing by winds in the western Atlantic was a better explanation of the phenomenon. Data used in these investigations were mainly from in situ measurements based on ship cruises. This method has limitations, as data collected is not extensive enough, in both time and space, to enable longer term studies of the upwelling. The continuous studies of the upwelling, particularly of its long-term variability, have been hindered by the lack of long-term observational data. The direct quantification of upwelling is often difficult as remote sensing of chlorophyll, which is a key signal, is often hampered by clouds. Upwelling indexes (e.g., [1] and [8]) have been used as proxies to quantify upwelling and to monitor changes in its intensity and spatial variability.

The availability of satellite-derived data has motivated our current objectives of understanding the variability of upwelling in the GoG. In this letter, we use mainly satellite-derived wind and SST data to understand the causal mechanism and derive indexes of the upwelling in the northwestern GoG (3° N–7° N, 10° W–4° E) during the period from 2003 to 2013.

II. Data and Methods

We use the multiscale ultrahigh resolution (MUR) SST analysis data set obtained from the NASA Jet Propulsion Laboratory (ftp://podaac-ftp.jpl.nasa.gov/allData/ghrsst/data/L4/GLOB/JPL/MUR/). This Level-4 data set spans from June 1, 2002 to present. The MUR data provide daily global SST at a spatial resolution of $0.01^\circ \times 0.01^\circ$ ($\sim$1 km $\times$ 1 km) by merging data from the Advanced Very High Resolution Radiometer (AVHRR), the Moderate Resolution Imaging Spectroradiometer (MODIS), and the Advanced Microwave Spectroradiometer-Earth observing system (AMSR-E). The merging is done by using an objective interpolation technique based on a wavelet decomposition to process each data set with respect to its inherent resolution [16], [17]. By merging different satellite products, the MUR data set takes advantage of the very high spatial resolution of infrared satellites (AVHRR and MODIS) and the better weather-tolerating microwave satellite (AMSR-E) to produce a 1-km very high resolution data (http://podaac.jpl.nasa.gov/dataset/JPL-L4UHfnd-GLOB-MUR?ids=&values=). Thus, the use of MUR SST data minimizes the effects of cloud coverage [18], which is a potential issue in the GoG.

Daily sea level anomaly data, available on a $0.25^\circ \times 0.25^\circ$ grid, is obtained from the Archiving, Validation, and Interpretation of Satellite Oceanographic data (AVISO) (http://www.aviso.oceanobs.com) [19]. This product is an optimal merging of sea-level data from multiple platforms: Ocean Topography Experiment (TOPEX)/Poseidon, Jason, European Remote Sensing Satellite (ERS-1/2), and Environmental Satellite (Envisat). These data are available from 1993 to present.

We use surface winds derived from the Quick Scatterometer (QSCAT) [20]. These data are available from August 1999 to October 2009 on a $0.25^\circ \times 0.25^\circ$ grid. We obtained weekly QSCAT data from http://apdrc.soest.hawaii.edu/las/v6/dataset?catitem=4169. We computed wind stress from wind speed using $\boldsymbol{\tau} = \rho_a C_d |\mathbf{U}| \mathbf{U}$, where $\boldsymbol{\tau}$ is the surface wind stress (units $= \mathrm{N \cdot m^{-2}}$), ρ_a is the air density (1.225 kg·m^{-3}), C_d is the drag coefficient (1.43×10^{-3}), and $\mathbf{U}$ is the wind speed in m·s^{-1} [21].

A monthly climatology for each data set is computed based on the available data for that variable during our study period of 2003–2013. We computed seasonal variations by subtracting the annual means from the monthly time series.

We obtained wind-driven upwelling estimates by computing Ekman transport $\mathbf{M}$, following the methods of [7] and [22], i.e.,

$$\mathbf{M} = \frac{\boldsymbol{\tau}}{\rho_o f} \tag{1}$$

(units $= \mathrm{m^2 \cdot s^{-1}}$), where ρ_o is the density of seawater (1024 kg·m^{-3}), and f is the Coriolis parameter ($2\Omega \sin \varphi$, where Ω is the angular velocity of the Earth and φ is the latitude).

The Ekman pumping velocity w_e was calculated from

$$w_e = \frac{1}{\rho_o f} \nabla \times \boldsymbol{\tau} \tag{2}$$

(units $= \mathrm{m \cdot s^{-1}}$), where $\nabla \times \boldsymbol{\tau}$ is the curl of the derived wind stress vector.

In order to compare the two upwelling estimates, we calculated a mean vertical velocity due to the offshore Ekman transport. We obtained this coastal divergence of the seaward Ekman current by dividing the Ekman transport by the Rossby radius of deformation R. The R determines the cross-shore length scale of active upwelling with the assumption of an idealized case of uniform alongshore winds, flat bottom topography, and no geostrophic adjustments [22], [23]. In the GoG coastal region, R is typically 70–100 km [24], [25]. We also obtained the net upwelling along the entire coastal region by summing up the transports due to the wind stress $(\mathbf{M})$ and the curl of the wind stress (W_e). This was done by first integrating $\mathbf{M}$ at every longitude, thus obtaining $\mathbf{M}$ in m^3 s^{-1}. We then integrated W_e to about 300-km offshore (i.e., the approximate distance offshore where the wind stress curl extends) and in each longitude, thus obtaining a vertical transport (m$^3 \cdot$ s^{-1}) that could be compared with the integrated $\mathbf{M}$ [14], [27]. Summarily, we are able to compare the relative contributions of the Ekman pumping and Ekman transport to the vertical velocities and transports in the coastal region.

We computed an upwelling index from the net transport as a fraction of the offshore transport perpendicular to the coast $(\mathrm{UI_{ET}})$. The $\mathrm{UI_{ET}}$ computation is based on the assumption that coastal upwelling is mainly due to the alongshore component of the wind acting in concert with the rotation of the Earth. Additionally, we obtained an SST upwelling index $(\mathrm{UI_{SST}})$ by computing the temperature difference between the coastal waters and the waters further offshore along the same longitude. These indexes are then used as a measure of the coastal upwelling intensity as a function of longitude and time [8], [27].

III. Results and Discussion

The annual mean and standard deviations of SST in the central Atlantic region are shown in Fig. 1(a). It is observed that SST is lowest along the equatorial region, east of 25° W. This is also the region of highest SST variability. In the northwestern

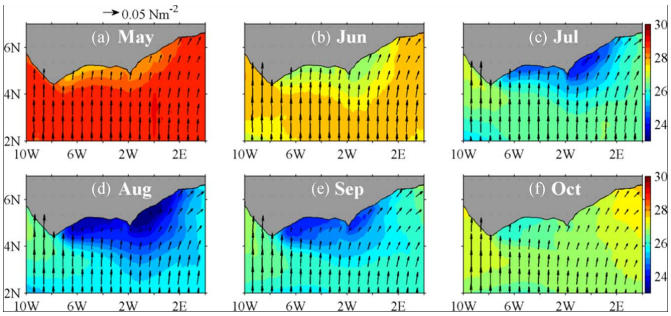

Fig. 2. Monthly mean SST (color shaded; in degrees Celsius) in the northwestern GoG region. Arrow vectors show mean wind stress ($\mathrm{N{\cdot}m^{-2}}$).

GoG region, SST standard deviations reach ∼0.5 °C with the annual mean plot suggesting relatively low SSTs along the coastal areas. The study region experiences significant SST variability on a seasonal time scale, and the temperatures could be ∼3 °C lower than the mean [see Fig. 1(b)]. At the beginning of the year, SST drops slightly, and this has been described as the minor upwelling season of the region [1], [6]. The SST then begins to rise, reaching a maximum during March–May. During boreal summer, between July and September, there is a significant drop in the SST, with the minimum SST occurring in August (see Fig. 1(b) and Fig. 2). This period is the major upwelling season [1], [3], [6]. The low SST is first noticeable in July, along the coasts of Ghana and Côte d'Ivoire with a core just east of Cape Three Points [see Fig. 2(c)]. By August, this patch of cool water spreads offshore and also further westward where it reaches Cape Palmas, the western limit of the GoG, and just off the coast of Côte d'Ivoire [see Fig. 2(d)]. Subsequently, the spread of this cooler water reduces during September, and then becomes warm again in November and December. The transition periods between cold and warm events can be attributed to the changes in winds that affect circulation in the GoG. During this time, there is advection of cold tongue waters by secondary circulation arising from Ekman transport when southeasterly winds respond to warm SST patches of tropical instability waves (TIWs; which are typically stronger to the north, around 3–5° N than the south), and partly by the south equatorial current (SEC) that further enhances the secondary circulation [28], [29]. Warm SST patches are formed with a threshold of 26–29 °C that increases wind speed during the development of the TIWs leading to enhanced wind stress curl. Perturbations of the curl generate perturbations in the Ekman pumping over the TIWs [28], [30].

In the northwestern GoG, the strongest wind stresses are observed in the boreal summer as a result of a strong trade wind system during this time [31], [32]. Closer to the coast, southwesterly winds are persistent east of 2° W. West of 2° W however, the winds are more southerly prior to the start of the boreal summer season. During the peak of summer, these winds tend to become more southwesterly, albeit weaker than is observed in the easternmost region of the study area (see Fig. 2). Because southerly winds are generally observed in the entire region for a large part of the year, there are limited areas along the coast where the local winds are favorably oriented to cause wind-driven upwelling (see Fig. 2). For example, along the coast of Ghana, winds are somehow parallel to the coast, particularly during the major upwelling season. The lack of predominantly upwelling favorable winds juxtaposed with the observation of low SSTs along the entire coastline of the region have led to suggestions that the upwelling occurs in the favorable subregions and then the local circulation advects this cooler waters to the other regions.

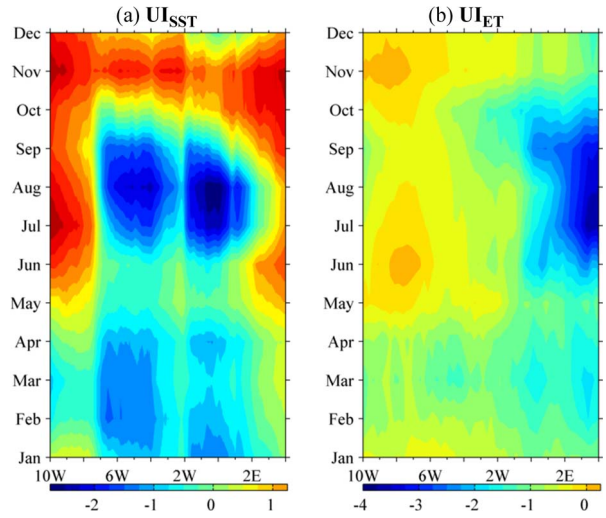

Fig. 3. Seasonal evolution of upwelling index computed from (a) difference between coastal and offshore SST ($\mathrm{UI_{SST}}$, °C) and (b) offshore Ekman transport ($\mathrm{UI_{ET}}, \mathrm{m^2 \cdot s^{-1}}$). A negative $\mathrm{UI_{SST}}$ indicates upwelling (coastal SST lower than offshore SST). A negative $\mathrm{UI_{ET}}$ indicates upwelling (offshore Ekman transport).

The SST-based upwelling index ($\mathrm{UI_{SST}}$) is able to capture the seasonal variability of the upwelling in the northwestern GoG [see Fig. 3(a)]. This is evidenced by the relatively high negative difference between the coastal SST and offshore SST during the beginning of the year (minor upwelling) and during boreal summer (major upwelling). Toward the end of the year, the $\mathrm{UI_{SST}}$ becomes strongly positive, indicating downwelling processes. The seasonality of coastal upwelling as obtained from the wind data ($\mathrm{UI_{ET}}$) is presented in Fig. 3(b). $\mathrm{UI_{ET}}$ suggests that Ekman transport occurs in several months in the year. This is a result of the southwesterly winds that are observed for several periods in the year [5], [31]. Additionally, the $\mathrm{UI_{ET}}$ computation assumes a transport that is perpendicularly oriented to the coastline, which is not entirely the situation in the study area. Furthermore, the Ekman theory assumption of a homogeneous ocean and constant wind does not allow the $\mathrm{UI_{ET}}$ to completely capture coastal upwelling around capes [8]. Nevertheless, the peak in this index coincides with the peak months of major upwelling in the region.

Generally, the $\mathrm{UI_{ET}}$ index shows that upwelling is strongest in the eastern half than western half of the study area. This could be caused by the stronger and more upwelling-favorable winds that occur east of 2° W (see Fig. 2). It is seen from the comparison of the upwelling indexes (see Fig. 3) that the time of occurrence of the peak of $\mathrm{UI_{SST}}$ coincided with the time of occurrence of the peak of the $\mathrm{UI_{ET}}$. The geographical locations of their peaks however do not coincide. Along the coast of the study area, the strongest upwelling-favorable winds are observed in the northeastern region, whereas the lowest SSTs occur just west of it (see Fig. 2). Further west, the favorable winds are weaker [see Fig. 2 and Fig. 3(b)], yet there is a substantial difference between the coastal and offshore SSTs. Thus, other

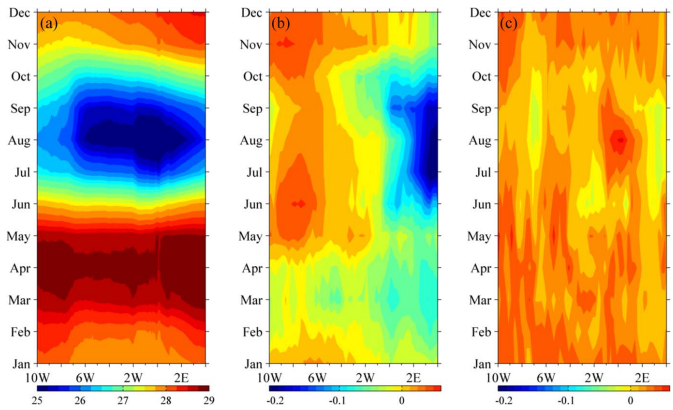

Fig. 4. Time-longitude plots (a) of SST (°C) averaged between 3° N–7° N. Contributions of (b) Ekman transport and (c) Ekman pumping to the vertical transport near the coast (in Sv).

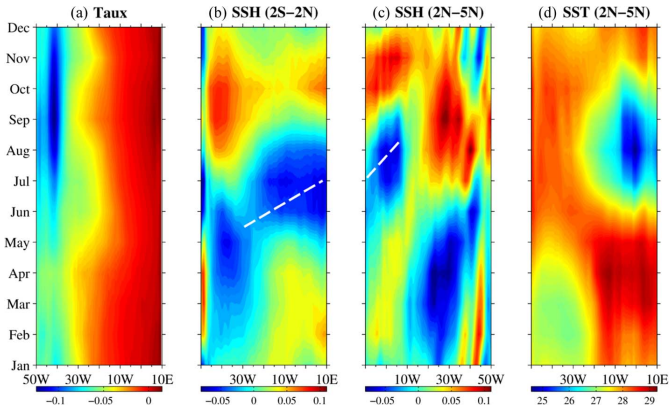

Fig. 5. Time-longitude plots of (a) mean zonal wind stress ($N \cdot m^{-2}$) averaged between 2° S–2° N. Sea level anomalies (in meters) averaged between (b) 2° S–2° N and (c) 2° N–5° N and (d) SST (°C) averaged between 2° N–5° N. The longitude axis in (c) has been reversed to show reflection at the eastern boundary. The white dashed lines represent propagation speeds of sea level anomalies.

factors than the winds should be considered in understanding the dynamics of the upwelling in this region. In summary, an upwelling index derived from offshore Ekman transport does not entirely reflect the dynamics in the study region and should be used with caution, most probably used together with the SST-derived upwelling index.

We examine the relative contributions of the winds to upwelling in the study region. Of the two processes, Ekman transport contributed more to upwelling than Ekman pumping. In Fig. 4, it is observed that low SSTs occupy the entire coastal region of the northwestern GoG during July–September. Corresponding strong upwelling-favorable Ekman transport and Ekman pumping velocity are however observed east of the prime meridian. West of ∼4° W, Ekman transport does not seem to support upwelling during the summer season. Peak positive wind stress curl (upwelling favorable) is observed during the summer, east of Cape Three Points. This is approximately the region with the coldest SSTs (see Fig. 2). West of this region, the wind stress curl is weaker and indeed tends to be negative around Cape Palmas during summer. It is worth mentioning that southwesterly winds are also observed along the entire coastal region during January–April, and this might be responsible for the positive pumping during this period [see Fig. 4(c)]. A corresponding upwelling-favorable Ekman transport was however absent during this period, particularly, west of Cape Three Points. A comparison of the vertical velocity implied by the Ekman transport with the Ekman pumping velocity (figure not shown) suggests that the net vertical velocity is driven more by the former process.

The SST cooling in the northwestern GoG coincides with the presence of westward winds in the western Atlantic Ocean [see Fig. 5(a)]. Consequently, we assess the remote contribution to upwelling in the northwestern GoG via equatorial waves propagation. During May–June, easterly winds begin to strengthen in the western Atlantic region [see Fig. 5(a)]. These enhanced winds will cause water to pile up against the western boundary and create a pressure gradient to balance the wind stress. Consequently, the winds excite upwelling Kelvin waves that propagate eastward along the equatorial region [see Fig. 5(b)]. The first and second baroclinic mode Kelvin waves propagate with phase speeds of ∼2.5 and 1.4 $m \cdot s^{-1}$, respectively [15], [33]. By July, the leading edge of the waves had reached the eastern coast, which bifurcate and propagate along the coast. The waves cause the thermocline to shoal and the sea level to drop [see Fig. 5(c)] and thereby aid an upwelling of cooler waters into the ocean surface [see Fig. 5(d)]. The arrival of the upwelling Kelvin waves in the study region coincides well with the time of occurrence of the peak low SST. These series of events as captured by the satellite-derived data are consistent with the numerical model simulations of some preceding authors [15], [34].

It is worth mentioning that other processes could augment the SST cooling observed in the study region. For example, the intensification of the Guinea Current during the boreal summer can influence the local upwelling via bathymetry and isothermal displacements resulting from local and remote wind forcing [1], [13]. Underneath this eastward flowing Guinea Current during the boreal summer is the westward flowing Guinea Undercurrent. The shear between these two currents enhances mixing, which aids surface SST cooling in the study region [13], [32].

IV. Summary and Conclusion

Studies of the upwelling phenomena in the northwestern GoG coastal region had resulted in various mechanisms to explain the dynamics [9], [10], [15]. Most of these studies were based on data collected from ships that did not allow for continuous measuring over a wider area and time. The availability of extensive satellite-derived data has allowed us to study the upwelling over a wider geographical region and time than would have from ship observations. Our use of the 0.01° × 0.01° (∼1 km × 1 km) high-resolution MUR SST data in this letter enabled the examination of finer scale structures that were not clearly delineated in other satellite products (e.g., AVHRR; figure not shown), possibly due to the issues of cloud coverage. Additionally, we found the seasonal cycle of SST to be relatively higher in the MUR data. This is consistent with the findings of [18] who used different SST products with different resolutions to study the SST gradients off the Peruvian coast, and concluded that the MUR data gave a better estimation of seasonal variability.

In this letter, we have quantified the relative contributions of wind processes to upwelling in the northwestern GoG. The

spatial distributions of the upwelling and the various processes have also been investigated. Upwelling in the region is typically noticed during January–March (minor upwelling) and July–September (major upwelling). The upwelling-favorable winds in the study area are relatively weaker than similar regions across the oceans [8], [22], [31]. This letter has found that Ekman transport contributed more to upwelling than Ekman pumping. Collectively however, both processes were not able to fully account for the upwelling in the region. The occurrence of peak upwelling and enhanced cooling east of $\sim 2^{\circ}$ W (Cape Three Points) suggests possible response of winds to SST patches of TIWs [28].

The consequence of the wind forcing on the ocean surface was analyzed in terms of the SST differences $(\mathrm{UI}_{\mathrm{SST}})$, which enabled us to quantify the spatial and temporal distribution of the upwelling. An attempt was made to derive similar index from the offshore Ekman transport $(\mathrm{UI}_{\mathrm{ET}})$, but that did not provide similar outcomes as the $\mathrm{UI}_{\mathrm{SST}}$. This discrepancy can be attributed to the lack of basin-wide upwelling-favorable winds in the northwestern GoG. It also supports the conclusion that upwelling in the region is not entirely under the influence of local winds, consistent with the observations of previous authors [5], [9], [15]. Spatially, the wind-driven upwelling was strongest in the eastern part of the study area, where favorable winds dominate. A high correlation was observed between the upwelling in the study region and the winds in the western equatorial Atlantic. Further investigation of this relationship showed that enhanced winds in the west excite equatorial and coastal wave processes that augment upwelling in the northwestern GoG coast. The Kelvin waves can be modulated by bathymetry to further enhance upwelling.

ACKNOWLEDGMENT

The authors would like to thank the various data sources for the freely available data (the MUR SST data were obtained from the NASA Jet Propulsion Laboratory at ftp://podaac-ftp.jpl.nasa.gov/allData/ghrsst/data/L4/GLOB/JPL/MUR/, the sea level anomaly data were obtained from http://www.aviso.oceanobs.com, and QSCAT wind products were obtained from http://apdrc.soest.hawaii.edu/las/v6/dataset?catitem=4169) and the Editor and anonymous reviewers whose comments significantly contributed to the improvement of this letter.

REFERENCES

[1] A. Bakun, "Guinea current upwelling," *Nature*, vol. 271, pp. 147–150, 1978.

[2] C. Roy, "The Cote d'Ivoire and Ghana coastal upwelling: Dynamics and changes," in *Dynamics and Use of Sardinella Resources From Upwelling Off Ghana and Ivory Coast*, F. X. Bard and K. A. Koranteng, Eds. Paris, France: ORSTOM, 1995, pp. 346–361.

[3] K. A. Koranteng "The impacts of environmental forcing on the dynamics of demersal fishery resources of Ghana," Ph.D. dissertation, Univ. Warwick, Coventry, U.K., 1998. [Online]. Available: www.oikos.warwick.ac.uk/ecosystems/ThesisArchive

[4] P. J. Lamb, "Case studies of tropical Atlantic surface circulation pattern during recent sub- Saharan weather anomalies, 1967–1968," *Mon. Weather Rev.*, vol. 106, pp. 482–491, 1978.

[5] D. Binet and J. Servain, "Have the recent hydrological changes in the Northern Gulf of Guinea induced the *Sardinella aurita* outburst?" *Ocean. Acta*, vol. 16, no. 3, pp. 247–260, 1993.

[6] G. Wiafe, H. B. Yaqub, M. A. Mensah, and C. L. J. Frid, "Impact of climate change on long-term zooplankton biomass in the upwelling region of the Gulf of Guinea," *ICES J. Mar. Sci.*, vol. 65, pp. 318–324, 2008.

[7] R. L. Smith, "Upwelling," *Oceanogr. Mar. Bio.—Annu. Rev.*, vol. 6, pp. 11–46, 1968.

[8] L. Nykjaer and L. Van Camp, "Seasonal and interannual variability of coastal upwelling along northwest Africa and Portugal from 1981 to 1991," *J. Geophys. Res.*, vol. 99, no. C7, pp. 14197–14207, Jul. 1994.

[9] M. C. Ingham, "Coastal upwelling in the Northwest Gulf of Guinea," *B. Mar. Sci.*, vol. 20, pp. 1–34, 1970.

[10] J. M. Verstraete, "The seasonal upwelling in the Gulf of Guinea," *Progress Oceanogr.*, vol. 29, no. 1, pp. 1–60, 1970.

[11] E. Marchal and J. Picaut, "Repartition et abundance evaluees par echo-integration des poissons du plateau Ivoiro-Ghaneen en relation avec les upwelling locaux," *J. Recherche Oceanographique*, vol. 2, pp. 39–57, 1977.

[12] J. Servain, J. Picaut, and J. Merle, "Evidence of remote forcing in the equatorial atlantic ocean," *J. Phys. Oceanogr.*, vol. 12, pp. 457–463, 1982.

[13] S. G. H. Philander, "Upwelling in the Gulf of Guinea," *J. Mar. Res.*, vol. 37, pp. 23–33, 1979.

[14] S. G. H. Philander, "The oceanic response to cross-equatorial winds (with application to coastal upwelling in low latitudes)," *Tellus*, vol. 33, pp. 204–210, 1981.

[15] D. Moore *et al.*, "Equatorial adjustment in the eastern Atlantic," *Geophys. Res. Lett.*, vol. 5, no. 8, pp. 637–640, 1978.

[16] T. M. Chin, R. F. Milliff, and W. G. Large, "Basin-scale, high-wavenumber sea surface wind fields from a multiresolution analysis of scatterometer data," *J. Atmos. Ocean. Tech.*, vol. 15, no. 3, pp. 741–763, 1998.

[17] T. M. Chin, J. Vazquez, and E. Armstrong, "A Multi-Scale, High-Resolution Analysis of Global Sea Surface Temperature," in *Algorithm Theoretical Basis Document*, Version 1.3. Pasadena, CA, USA: Jet Propulsion Laboratory, 2013.

[18] J. Vazquez-Cuervo *et al.*, "An analysis of SST gradients off the Peruvian coast: the impact of going to higher resolution," *Remote Sens. Environ.*, vol. 131, pp. 76–84, Apr. 2013.

[19] N. Ducet, P.-Y. LeTraon, and G. Reverdin, "Global high resolution mapping of ocean circulation from TOPEX/Poseidon and ERS-1/2," *J. Geophys. Res.*, vol. 105, no. C8, pp. 477–498, Aug. 2000.

[20] W. T. Liu, "Progress in scatterometer application," *J. Oceanogr.*, vol. 58, no. 1, pp. 121–136, 2002.

[21] R. H. Weisberg and C. Wang, "Slow variability in the equatorial west-central Pacific in relation to ENSO," *J. Clim.*, vol. 10, pp. 1998–2017, 1997.

[22] M. H. Pickett and J. D. Paduan, "Ekman transport and pumping in the California Current based on the U.S. Navy's high-resolution atmospheric model (COAMPS)," *J. Geophys. Res.*, vol. 108, no. C10, pp. 3327, 2003.

[23] J. S. Allen, "Upwelling and coastal jets in a continuously stratified ocean," *J. Phys. Oceanogr.*, vol. 3, no. 3, pp. 245–257, Jul. 1973.

[24] D. Adamec and J. J. O'Brien, "The seasonal upwelling in the Gulf of Guinea due to remote forcing," *J. Phys. Oceanogr.*, vol. 8, no. 6, pp. 1050–1060, Nov. 1978.

[25] C. Colin, "Coastal upwelling events in front of the Ivory Coast during the FOCAL Program," *Oceanol. Acta*, vol. 11, no. 2, pp. 125–138, 1988.

[26] R. M. Castelao and J. A. Barth, "Upwelling around Cabo Frio, Brazil: The importance of wind stress curl," *Geophys. Res. Lett.*, vol. 33, no. 3, Feb. 2006, Art. ID. L03602.

[27] I. Alvarez *et al.*, "Comparative analysis of upwelling influence between the western and northern coast of the Iberian Peninsula," *Cont. Shelf Res.*, vol. 31, no. 5, pp. 388–399, Apr. 2011.

[28] I. Muhammed, "The effect of large-scale interannual variations in the Gulf of Guinea," Ph.D. dissertation, Univ. Southampton, Southampton, U.K., 2011. [Online]. Available: http://eprints.soton.ac.uk/209795/

[29] H. Seo and S. P. Xie, "Response and impact of equatorial ocean dynamics and tropical instability waves in the tropical Atlantic under global warming: A regional coupled downscaling study," *J. Geophys. Res.*, vol. 116, no. C3, p. 3026, Mar. 2011.

[30] D. B. Chelton *et al.*, "Observations of coupling between surface wind stress and sea surface temperature in the eastern tropical Pacific," *J. Clim.*, vol. 14, no. 7, pp. 1479–1498, 2001.

[31] R. W. Houghton, "Influence of local and remote wind forcing in the Gulf of Guinea," *J. Geophys. Res.*, vol. 94, no. C4, pp. 4816–4828, Apr. 1989.

[32] R. W. Houghton, "Circulations and hydrographic structure of the Ghana continental shelf during the 1974 upwelling," *J. Phys. Oceanogr.*, vol. 6, no. 6, pp. 909–924, Nov. 1976.

[33] D. Moore and S. G. H. Philander, "Modelling of the tropical oceanic circulation," *The Sea*, vol. 6, E. Goldberg *et al.*, Eds. Hoboken, NJ, USA: Interscience-Wiley, 1977, pp. 319–361.

[34] J. J. O'Brien, D. Adamec, and D. W. Moore, "A simple model of upwelling in the Gulf of Guinea," *Geophys. Res. Lett.*, vol. 5, no. 8, pp. 641–644, Aug. 1978.